

Efficiency estimation of four different atmospheric correction algorithms in a sediment-loaded tropic lake for Landsat 8 OLI sensor

Daniel Schaffer Ferreira Jorge¹

Diogo de Jesus Amore¹

Claudio Clemente Faria Barbosa¹

¹National Institute for Space Research
Caixa Postal 515 - 12227-010 - São José dos Campos - SP, Brasil
{danielsfj,amore}@dsr.inpe.br
claudio@dpi.inpe.br

Abstract. Atmospheric correction algorithms allow the reduction of atmospheric components influence in the acquisition of earth's surface reflectance properties. Quantifying this reduction is critical for the remote sensing science. Different regions have different natural or man-made composition and respond differently for each algorithm. Highly turbid inland waters are significantly sensitive to atmospheric correction algorithms, and these waters must be evaluated with care. This paper investigated the impact of turbidity levels in a sediment-laden tropical lake through the correlation analysis between image and ground-based Remote Sensing reflectance (Rrs) for the Landsat 8 OLI sensor. Four atmospheric algorithms were tested for Rrs estimation: DOS (Dark Object Subtraction), FLAASH (Fast Line-of-sight Atmospheric Analysis of Spectral Hypercubes), 6S (Second Simulation of the Satellite Signal in the Solar Spectrum) and QUAC (QUick Atmospheric Correction). A regression linear model was applied to the data, and results showed two distinguishable features within the samples. The first feature set presents a near-one higher-angle slope value with R^2 values ranging from 49-64%, and a near-zero lower-angle slope with R^2 ranging from 49-71%. Despite the small data set used in this work, it is reasonable to assume the results demonstrate that, during the atmospheric correction process, the Rrs correlation undergoes a slope direction change. This is most likely due to the influence of higher turbidity levels.

Keywords: water constituents, optically complex waters, atmospheric correction, calibration, validation, remote sensing

1. Introduction

The water superficial color, or spectral reflectance, is a result of interactions between optically active components (OAC) present in water via absorption and scattering processes (Preisendorfer, 1961) with solar irradiance within the visible region of the electromagnetic spectrum (400 a 700 nm). Reflectance is directly proportional to light scattering towards the surface, and inversely proportional to the absorption coefficient (Morel & bricaud, 1981; Gordon, 1991), which allows the use of reflectance measurements acquired via remote sensing to obtain information on the water optically active constituents (Gordon et al., 1989). In case I waters, the absorption coefficient is directly influenced by phytoplankton (a_{ph}), whereas the influence of colored dissolved organic matter (CDOM), detritus and sediment vary only with chlorophyll-a concentration (Preisendorfer, 1961; Morel & Maritorena, 2001; Morel & Gentili 2009). In optically complex environments (Case II waters), CDOM and detritus absorption coefficients tend toward higher values than $a_{ph}(\lambda)$ within the visible blue and red spectral regions (Galegos & Neale, 2002).

Since the launch of the first remote sensing sensor, the scientific community spent a great effort increasing their radiometric and spectral performance. Nevertheless, processing ocean color data for optically complex waters remains a challenging task. This is mainly caused by the high CDOM and detritus concentration (Siegel et al., 2000), reducing the precision of the atmospheric correction process, with misleading measurements. These normally result in distortion of the actual reflectance of the objects which subsequently affects the extraction of information from images. Deciding on the need to correct for atmospheric effects is often a critical first step that can affect subsequent steps in satellite

data applications. In case I waters, it is assumed that seawaters absorbs all the light in the red and near-infrared (NIR) region of the spectrum, referred as the black-pixel assumption (Gordon & Wang, 1994). This allows estimating the contribution of the atmosphere and subsequently the light scattered by the water column and measured by the satellite. While the black-pixel assumption is verified in clear ocean waters, it induces significant errors when applied in optically complex waters. Moreover, these environments present high spatial and temporal variability reducing the performance of global parameterizations (e.g., Loisel et al., 2010; Werdell et al., 2007) and significant errors remain in retrieving water properties from satellite remote sensing (e.g., Zibordi et al., 2009a, 2009b).

Numerous atmospheric correction algorithms were developed taking into account non-negligible NIR water contribution to the measured signal. A regional validation of these algorithms is required to gain insight in their performances and limitations and to aid the retrieval of precise radiometric data. Despite several studies compared the performances of new developed algorithms against the standard atmospheric correction algorithms for ocean water (e.g., Kuchinke et al., 2009; Ruddick et al., 2000; Wang & Shi, 2007; Wang et al., 2009), only few studies were made for optically complex waters, with a focus on the algorithm performance and not in the comparison of multiple atmospheric correction algorithms. This paper aims to cover that gap.

2. Materials and Methods

2.1 Study area

The Amazon basin drains a surface area of around 6,000,000 km², constituting ca. 5% of the Earth's terrestrial surface. The Amazon River and its large tributaries are accompanied along their middle and lower courses by large 'várzeas' which cover an area of about 300,000 km² (Junk, 1997), including 110,000 km² in the main stream (Melack and Fisher, 1990). Permanent and temporary lakes increase in size and become connected to each other during high river discharge. The 'Várzea do Lago Grande de Curuai' (Fig. 1) has a flood area that varies between 1340 and 2000 km² (Kosuth, 2002), according to the flow period. Its watershed covers 3660 km², including open water areas. The 'Várzea do Lago Grande de Curuai' is comprised of several white-water lakes (waters characterized by high suspended sediment loads) and black-water lakes (waters characterized by high concentrations of dissolved humic acids and low concentrations of suspended sediment) interconnected with each other and permanently connected to the Amazon mainstream by different small channels. The major lake, 'Lago Grande de Curuai', is a white-water lake, ca. 359 km², located between 56°00'W (upstream) and 55°03'W (downstream) and 2°17'S and 1°55'S. This lake is permanently linked to Amazon river by two channels 'Foz Sul' (FS) and 'Foz Norte' (FN) (Fig. 1).

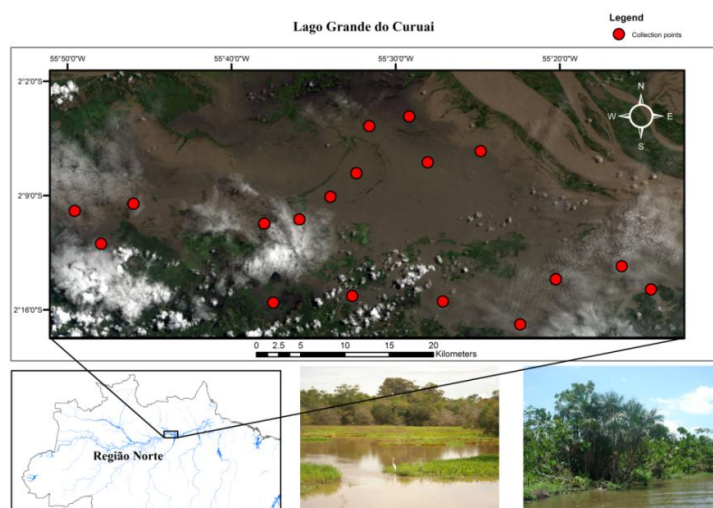


Figure 1. Map of the study area (Lago Grande do Curuai). Red circles represent the *in situ* radiometric data collected.

2.2 Image/Sensor

Landsat 8/OLI was launched on February 11, 2013 and normal operations started on May 30, 2013. It has a ground track repeat cycle of 16 days with an equatorial crossing time at 10:00 a.m. The Operational Land Imager (OLI) on L8 is a nine band push broom scanner with a swath width of 185 km, eight channels at 30 m and one panchromatic channel at 15 m spatial resolution. Compared to the Thematic Mapper (L4-5/TM) and the Enhanced Thematic Mapper Plus (L-7/ETM+) carried on previous Landsat missions, L8/OLI offers higher signal-to-noise ratios (SNR), mainly because of longer integration times on the push broom scanner, and a better radiometric resolution (12 instead of 8 bits for radiometric digitization) and spectral resolution (additional band for coastal/aerosol centred at 443 nm). A single orthorectified and terrain corrected Level 1T OLI image was obtained from USGS EarthExplorer (<http://earthexplorer.usgs.gov/>) for the Curuai Lake. In this study, the reflectance was calculated for each spectral band using ENVI software for radiometric calibration.

2.3 Atmospheric correction

2.3.1 Dark Object Subtraction

Dark object subtraction searches each band for the darkest pixel value. Assuming that dark objects reflect no light, any value greater than zero must result from atmospheric scattering. The scattering is removed by subtracting this value from every pixel in the band. This simple technique is effective for haze correction in multispectral data, but it should not be used for hyperspectral data (Chavez Jr., 1988).

2.3.2 FLAASH

FLAASH (Fast Line-of-sight Atmospheric Analysis of Spectral Hypercubes) is a MODTRAN-based “atmospheric correction” software package which was developed to support current and planned IR-visible-UV hyperspectral and multispectral sensors. The main objectives are to provide (1) accurate, physics-based derivation of surface and atmospheric properties (such as surface albedo, surface altitude, water vapor column, aerosol and cloud optical depths, surface and atmospheric temperatures), (2) minimal computation time requirements, and (3) an interactive, user-friendly interface for running arbitrary MODTRAN calculations. FLAASH is written in the Interactive Data Language (IDL) for compatibility with a wide variety of computer platforms and to facilitate its use with IDL-based display/analysis software such as ENVI. FLAASH incorporates MODTRAN4 radiation

transfer code. Any of the standard MODTRAN model atmospheres and aerosol types can be chosen to represent the scene, and a MODTRAN solution is computed for each image. FLAASH also includes correction for adjacency effect, an option to compute a scene-average visibility, uses the most advanced techniques for handling particularly stressing atmospheric conditions (such as the presence of clouds), and cirrus and opaque cloud classification map (Cooley et al., 2002).

2.3.3 6S

The Second Simulation of the Satellite Signal in the Solar Spectrum (6S) is a radioactive transfer code developed by Vermote et al. (1997a), following earlier versions developed by Tanré et al. (1990). Given the target reflectance of a pixel and the sensor characteristics, the code simulates the effect of the atmosphere in the signal due to scattering by molecules and aerosols, and absorption - mainly by H₂O, CO₂, O₂, O₃, CH₄, N₂O and CO (Vermote et al. 1997b). The 6S RTC can also be run in the 'atmospheric correction mode', computing in this case the Bottom of Atmosphere (BOA) reflectance, given the at-sensor measured value. The main limitations to the operational use of the 6S code is the difficulty in getting the required atmospheric parameters and the computational time involved in running the code on a pixel-by-pixel basis (Zhao et al. 2000).

2.3.4 QUAC

QUAC (QUick Atmospheric Correction) determines atmospheric correction parameters directly from the observed pixel spectra in a scene, without ancillary information. It is based on the empirical finding that the average reflectance of diverse material spectra is not dependent on each scene, so processing is much faster compared to first-principles methods. QUAC also allows for any view angle or solar elevation angle, if a sensor does not have proper radiometric calibration or the solar illumination intensity is unknown (with cloud decks, for example) (Bernstein et al., 2012).

2.5 *In situ* Data

Radiometric data for validation purposes were collected from eighteen points across the Lago grande do Curuai. The points were spaced from one another a distance of 5 km minimum and 60 km maximum. Six RAMSES TRIOS sensors were used to collect electromagnetic radiation in six distinct positions, upwelling radiance, downwelling irradiance and downwelling radiance inside the water; water leaving radiance (45°), sky radiance (45°) and downwelling irradiance outside the water. Fairly clear sky conditions were achieved during measurements despite the fact that cloud cover is high for the area. Raw data were processed to Remote Sensing reflectance (R_{rs}) in order to establish a correlation with reflectance data from the atmospherically corrected images.

2.6 Statistics and Linear Regression

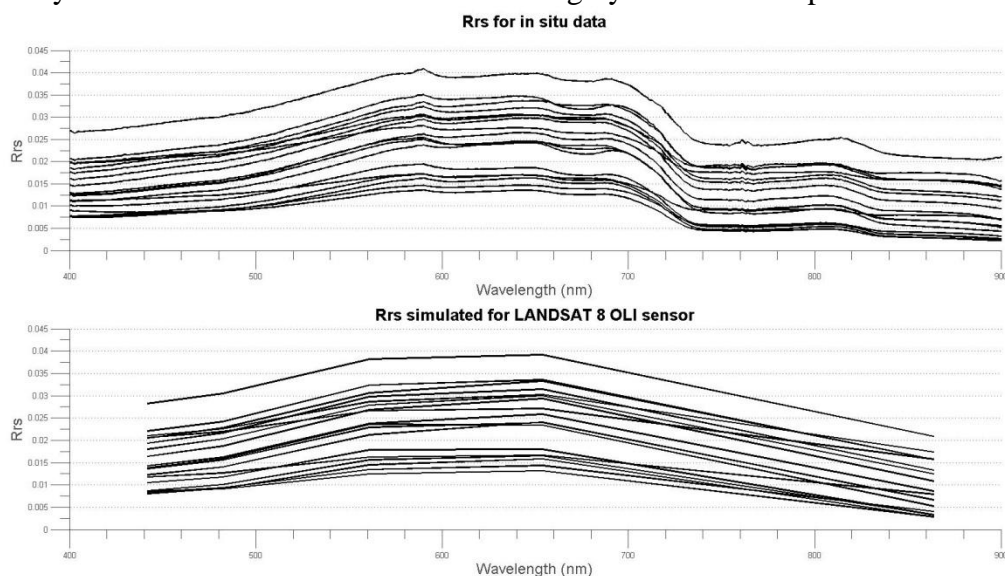
The coefficient of determination (R^2) was calculated to investigate the relationship between the image data and ground-based radiometric data. R^2 describes the proportion of variance of the dependent variable explained by the regression model. It is a measure of the Sum of Squares Regression over the Sum of Squares Total (Regression and Error). The regression coefficient (fitted curve slope) was also calculated in order to evaluate the rate of change of the image R_{rs} with respect to that of in-situ-calculated R_{rs}.

3. Results and Discussion

3.1 *In situ* water spectra

In order to understand lago grande do Curuai optical behavior, the R_{rs} spectra for the *in situ* dataset and simulated OLI dataset can be observed in the Figure 2. In the first graph, three distinct features can be identified. In the first feature, between 400 and 580, there is a

linear increase in the R_{rs} magnitude, characteristic of optical conditions of mixed waters, in which the dominance of either phytoplankton, CDOM or sediments cannot be identified (SISWANTO et al, 2012), from 580 to 700 nm there is a plateau, characteristic of waters with high sediment concentration (KUTSER et al, 2006), and in the 740 to 900 nm range, the R_{rs} spectra is dominated by water absorption, and linear sediment backscattering, with a small peak in 850 nm. In the second graph, a spectral transformation was applied using the sensor impulse function. One can observe that the first two features were maintained from the original hyperspectral *in situ* data, whereas the third one changed to a linear decrease, caused by the lack of higher-resolution spectral bands. Overall, OLI-simulated R_{rs} spectra successfully maintained the distinct features of a highly turbid water spectrum.



Figur 2. Spectral behavior for each collected point per unit of steradian (sr^{-1}) and nanometer (nm). The upper graph represent the *in situ* measurements every 1 nm. The lower graph display the sensor adjusted *in situ* measurement.

During the development of atmospheric correction algorithms for ocean color, the NIR range have been used as a proxy for atmospheric scattering, assuming that all signal identified in that range is caused by it. Although this statement is valid for clear ocean waters, in coastal and inland waters it is possible to identify the high sediment backscattering coefficient influence in the R_{rs} spectra, especially for highly turbid waters such as in lago grande do Curuai. This occurs as a linear increase in the R_{rs} magnitude for whole spectra. This behavior can be observed in figure 2, in which the simulated R_{rs} in the NIR range is not as low as it was expected (near zero). Hence, the R_{rs} derived from satellite data in the NIR is caused by the sum of the signal from the sediment backscattering and atmospheric scattering.

Atmospheric corrections that simply remove the signal estimated from the NIR (e.g. DOS and QUAC) may underestimate the R_{rs} provenint from highly turbid waters, whereas atmospheric corrections algorithms that focus on SWIR bands (e.g. FLAASH) or atmospheric absorption and scattering properties (e.g. 6S) may reduce this shortcoming.

3.2 Estimated water spectra

Figures 3 and 4 show the linear regression model result. The scatterplots for each atmospheric correction algorithm were split into two. This was performed due to the identification of two different patterns within the initial results. However, this was not achieved by an analysis of covariance due to lack of sampled data. Therefore, an empirical split of the scatterplot data allowed the separation and further statistical computation of the two patterns.

Figure 4 depicts the scatterplots for each band with lower slope values. The discrepancy in the slope magnitude indicates lower correlation between the two datasets. This means that despite the variation within the *in situ* Rrs, not much variation can be observed in the image Rrs. This set of data in Figure 4 might be influenced by an external parameter that cannot be identified with these set of *in situ* radiometric data only. The most likely parameter is the turbidity level since the area of study is a highly turbid optically complex case II water.

Oppositely, R^2 value for figure 4 is reasonably similar to that of figure 3. This indicates that the data variance for the figure 4 dataset are similar to that of figure 3, and both figures indicate that the dependent variable (image Rrs) variance is explained by the model with some degree of certainty, considering the number of samples collected for this study. A further analysis of figures 3 and 4 also expose how the longer wavelengths OLI bands tend to generate higher R^2 values for the lower-angle slope.

Several atmospheric algorithms specific for turbid waters were developed (Ruddick et al, 2000). These algorithms reconsider the assumption that there is negligible water-leaving radiance at 670 nm. This allows for the more accurate generation of atmospherically corrected images for turbid waters. Since the algorithms used in this work were not specific for turbid waters, inaccuracies were expected to appear. Hence, figure 4 might represent the result of these inaccuracies due to its low slope angle.

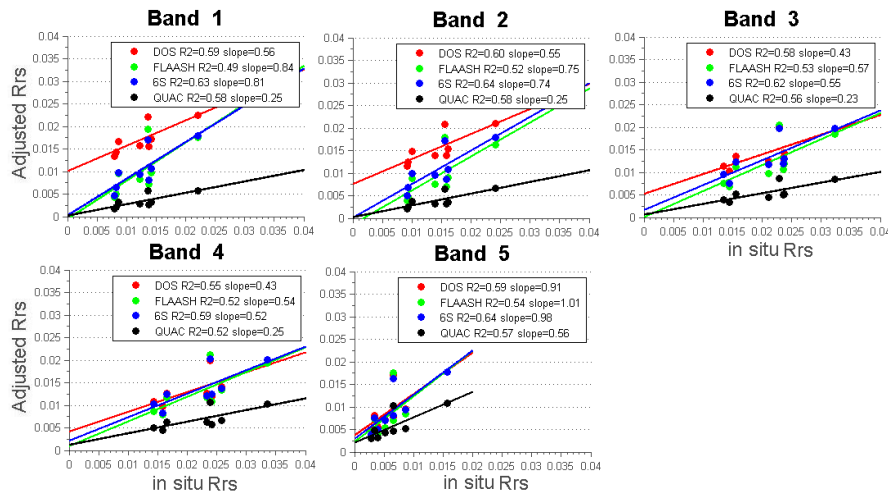


Figure 3. First feature set empirically selected showing a higher correlation between the image Rrs and ground-based Rrs per unit of steradian (sr^{-1}).

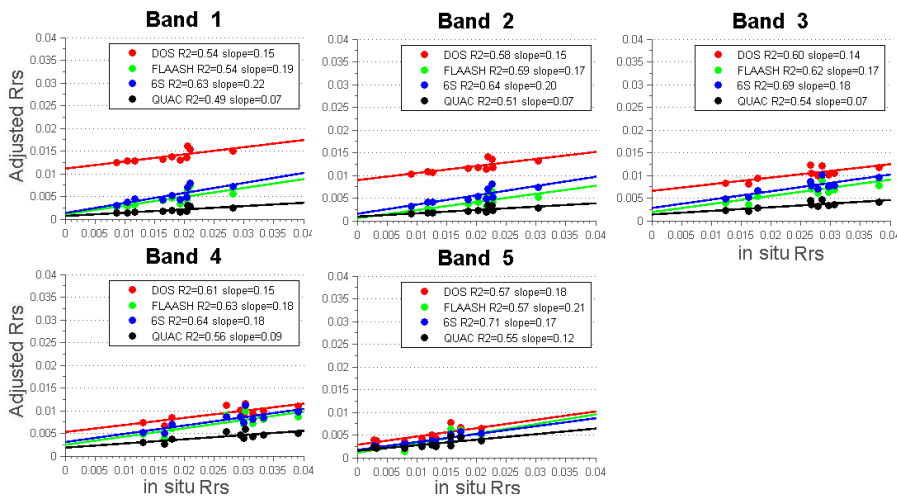


Figure 4. Second feature set empirically selected showing a lower correlation between the image Rrs and ground-based Rrs per unit of steradian (sr^{-1}).

When taking into account the assumptions made for each atmospheric model, it was expected a shift in the linear model slope due to the increase of sediment concentration. This concentration influenced the Rrs spectra in two distinct aspects: on its shape and magnitude. Regarding the atmospheric correction, the magnitude was critical for precise Rrs estimation. An increase in sediment concentration had a linear impact on the Rrs spectra, increasing the Rrs magnitude for both visible and NIR wavelengths. Hence, the atmospheric correction algorithms using the NIR as atmospheric scattering baseline, underestimated Rrs, as observed in the fitted model slope decrease from figure 3 to figure 4. Although the shift coincided with the theoretical background for turbid waters, this work lacks *in situ* measurements of sediment concentration for a more robust matching conclusion.

4. Conclusion

Atmospheric correction algorithms are essential for an accurate acquisition of Earth surface water optical information. This paper investigated the impact of turbidity levels in a sediment-loaded tropical lake for the Landsat 8 OLI sensor through the comparison of four well established atmospheric correction algorithms. The regression linear model applied on the data showed two distinguishable features within the sample distribution. The first feature set presented a near-one higher-angle slope value, and the second one showed a near-zero lower-angle slope. The results demonstrated that during the atmospheric correction process the samples underwent a slope direction change. Sediment concentration increase might be the main factor in the underestimated results found in all correction models.

FLAASH and 6S were more accurate for this specific dataset. QUAC showed the worst correlation results, underestimating the image Rrs for all collected points whereas DOS overestimated them. This work showed preliminary results in regional scale for each atmospheric model in an optically complex environment. However, care must be taken while extrapolating these results for other areas. Despite the preliminary results found, this is a novel work attempting to evaluate atmospheric correction for Landsat OLI sensor. Future studies validating these algorithms should consider the acquisition of *in situ* data for sediment concentration levels and composition. Moreover, the authors suggest applying this methodology in other study sites with different optical composition.

5. References

- Bernstein, L.S.; Jin, X.; Gregor, B.; Adler-Golden, S.M. Quick atmospheric correction code: algorithm description and recent upgrades. **Optical Engineering**, v.51, n.11, 2012.
- Chavez, Jr., P.S. An improved dark-object subtraction technique for atmospheric scattering correction of multispectral data. **Remote Sensing of Environment**, v.24, p.459-479, 1988.
- Cooley, T.; Anderson, G.P.; Felde, G.W.; Hoke, M.L.; Ratkowski, A.J.; Chetwynd, J.H.; Gardner, J.A.; Adler-Golden, S.M.; Matthew, M.W.; Berk, A.; Bernstein, L.S.; Acharya, P.K.; Miller, D.; Lewis, P. FLAASH, a MODTRAN4-based atmospheric correction algorithm, its application and validation. **Geoscience and Remote Sensing**, 2002
- Gallegos, C.L.; Neale, P.J. Partitioning spectral absorption in case 2 waters: discrimination of dissolved and particulate components. **Applied Optics**, v.41, p.4220-4233, 2002.
- Gordon, H. R. Dependence of the diffuse reflectance of natural waters on the Sun angle. **Limnology and Oceanography**, v.34, p.1484-1489, 1989.
- Gordon, H.R. Absorption and scattering estimates from irradiance measurements: Monte Carlo simulations. **Limnology and Oceanography**, v.36, p.769-777, 1991.
- Junk, W.J. The Central Amazon Floodplain: ecology of a pulsing system. **Ecological Studies**, v. 126. 525 pp. 1997

- Junk, W.J.; Piedade, M.T.F. Plant life in the floodplain with special reference to herbaceous plants. In: Junk, W.J. (Ed.), **The Central Amazon Floodplain: Ecology of a Pulsing System**, Ecological Studies, vol. 126, 1997, pp. 147–185.
- Kosuth, P. A case study of floodplains dynamics: dynamics, water balance, sediment balance of the Várzea of Lago Grande de Curuai. **Second LBA Conference**, 7–10 July, Manaus, Brazil, 2002.
- Kuchinke, C.P., Gordon, H.R., & Franz, B.A. Spectral optimization for constituent retrieval in Case 2 waters I: Implementation and performance. **Remote Sensing of Environment**, 113/3, 571-587, 2009.
- Kutser, T.; Metsamaa, L.; Strömbeck, N.; Vahtmäe, E. Monitoring cyanobacterial blooms by satellite remote sensing. **Estuarine Coastal Shelf Science**, v.67, p.303–312, 2006.
- Loisel, H., Lubac, B., Dessailly, D., Duforet-Gaurier, L., & Vantrepotte, V. Effect of inherent optical properties variability on the chlorophyll retrieval from ocean color remote sensing: An in situ approach. **Optics Express**, 18, 20949–20952, 2010.
- Melack, J.M.; Fisher, T.R. Comparative limnology of tropical floodplain lakes with an emphasis on the central Amazon. **Acta Limnologica Brasiliensia** v.3, 1990, p.1 – 48.
- Morel, A.; Bricaud, A. Theoretical results concerning light absorption in a discrete medium, and application to specific absorption of phytoplankton. **Deep-Sea Research**, v.28, p.1375-1393, 1981.
- Morel, A.; Maritorena, S. Bio-optical properties of oceanic waters: A reappraisal. **Journal of Geophysical Research**, v.106, p.7763-7780, 2001.
- Morel, A. & Gentili, B. A simple band ratio technique to quantify the colored dissolved and detrital organic material from ocean color remotely sensed data. **Remote Sensing of Environment**, 113, 998-1011, 2009.
- Preisendorfer, R. W. Application of radiative transfer theory to light measurements in the sea. In: **IUGG-IAPO Symposium on Radiant Energy in the Sea**, 4-5 Aug. 1960, Helsinki: Finland. Monograph N.10, p.83-91, 1961.
- Ruddick, K. G.; Ovidio, F.; Rijkeboer, M. Atmospheric correction of SeaWiFS imagery for turbid coastal and inland waters. **Applied Optics**, v.39, n.6, p.897-912, 2000.
- Siswanto, E.; Ishizaka, J.; Tripathy, S.C.; Miyamura, K. Detection of harmful algal blooms of *Karenia mikimotoi* using MODIS measurements: A case study of Seto-Inland Sea, Japan. **Remote Sensing of Environment**, v. 129, p.185-196, 2013.
- Vermote, E.F.; Tanre, D.; Deuze, J.L., Herman, M.; Morcrette, J.J. Second Simulation of the Satellite Signal in the Solar Spectrum, 6S: An Overview. **IEEE Transactions on Geoscience and Remote Sensing**, v.35, n.3, 1997.
- Vermote, E. F., Tanre, D., Deuze, Herman, M. and Morcrette, J. Second simulation of the satellite signal in the Solar Spectrum, 6S: An overview. **IEEE Transactions on Geoscience and Remote Sensing**, 35, 1997b, pp. 675-686.
- Wang, M., Son, S., & Shi, W. Evaluation of MODIS SWIR and NIR-SWIR atmospheric correction algorithms using SeaBASS data. **Remote Sensing of Environment**, 113, 635–644, 2009.
- Werdell, P. J., Franz, B. A., Bailey, S. W., Harding, L. W., Jr., & Feldman, G. C. Approach for the long-term spatial and temporal evaluation of ocean color satellite data products in a coastal environment. **Proceeding of SPIE**, Vol. 6680. (pp. 12), 2007.
- Zhao, W., Tamura, M., and Takahashi, H. Atmospheric and Spectral Corrections for Estimating Surface Albedo from Satellite Data Using 6S Code. **Remote Sensing of Environment**, v.76, p.202-212, 2000.
- Zibordi, G., Berthon, J.-F., Mélin, F., D'Alimonte, D., & Kaitala, S. Validation of satellite ocean color primary products at optically complex coastal sites: Northern Adriatic Sea, Northern Baltic Proper and Gulf of Finland. **Remote Sensing of Environment**, 113, 2574–2591, 2009.
- Zibordi, G., Mélin, F., Berthon, J., Holben, B., Slutsker, I., Giles, D., D'Alimonte, D., Vandemark, D., Feng, H., Schuster, G., Fabbri, B.E., Kaitala, S. & Seppälä, J. AERONET-OC: A Network for the Validation of Ocean Color Primary Products. **J. Atmos. Oceanic Technol.**, 26, 1634–1651, 2009.